# SIMULATION OF HIGH ALTITUDE FLIGHT IN WIND-TUNNELS AND CORRELATION OF FREE-FLIGHT AND WIND TUNNEL DATA

W. Wuest

DFVLR-AVA Institut für Dynamik verdünnter Gase
3400 Göttingen, Bunsenstrasse 10, West Germany

## Abstract

The flight in high altitudes is generally associated with high speed and consequently high stagnation temperatures because of the limitations given by the " flight corridor". Wind tunnel simulation of high altitude and high enthalpy flight is faced with following problems: a) Rarefaction effects on the pressure distribution and hence on the forces are different for slender and blunt bodies. Realistic lifting bodies are generally composed of both elements and consequently Mach number as well as Reynolds number must be duplicated. b) Correct wind tunnel simulation of the complete nonequilibrium and high enthalpy flow field past lifting reentry vehicles under conditions of interest appears to be impossible. Techniques involving incomplete simulation must be employed. c) Only scarce free flight data are available for hypersonic high Reynolds number flight in equilibrium regime; no data are available for nonequilibrium regime. d) This situation requires an intensification of further theoretical study of viscous nonequilibrium flows past complex three dimensional shapes with the aim to support incomplete wind tunnel simulation.

## 1. Introduction

The flight at high altitudes is determined by the ⟨⟨ flight corridor ⟩⟩, which bounds the possible flight regime with sufficient lift force and maximum heat load. It is generally associated with high velocity and consequently high stagnation enthalpy, low density, and real gas effects. The flight conditions of hypersonic high altitude flight may be simulated rather satisfactorily in different types of hypersonic wind tunnels, such as shock tubes and Ludwieg tube tunnels for the continuous regime and hypersonic low density tunnels or molecular beam arrangements for the transitional and free molecular flow regime. With increasing rarefaction, however, severe problems may be encountered.

a) The hypersonic similarity law for inviscid flows is no longer valid because viscous effects predominate, which are intensifying with increasing rarefaction. Rarefaction effects are different for slender and blunt bodies; as lifting bodies are generally composed of both elements, a complete simulation of Mach- and Reynolds number is needed.

b) The combined action of rarefaction and high enthalpy causes relaxating nonequilibrium flow. These phenomena are different in free flight and in wind tunnel flow and possible discrepancies of experimental data must be considered.

c) The difficulties preventing full wind tunnel simulation of the flight corridor, namely reservoir temperature and pressure requirements and also effects of chemical and vibrational freezing in wind tunnel nozzles, appear at present to be insuperable. Reliance must be placed on non-simulating wind tunnel tests coupled with extensive computation. In what follows the different problems are discussed in detail comparing wind tunnel and free flight data with theoretical results.

## 2. Mach- and Reynolds number simulation

### 2.1 Flight corridor and Mach-Reynolds number regime

The flight conditions of a hypersonic vehicle may not be adequately defined by altitude and velocity but rather in a corresponding Mach-Reynolds number chart. Typical flight conditions of various hypersonic vehicles are shown in an altitude-velocity diagram (Fig. 1) and in the corresponding

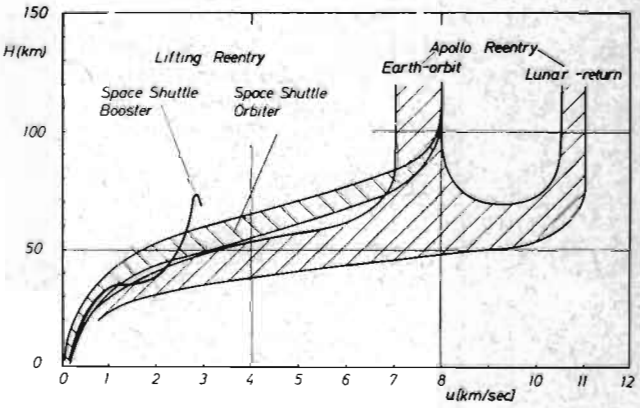


Fig. 1. Flight trajectories of typical re-entry vehicles (Altitude H versus velocity v)

Mach-Reynolds number chart (Fig. 2). In the latter chart the different regimes of rarefaction may be indicated and the boundaries are characterized by the ratio of the mean free path and a characteristic length. In the near continuum regime this length is given by the boundary layer thickness and rarefaction effects are therefore characterized by the well known similarity parameter $Ma_\infty/\sqrt{Re_\infty}$.

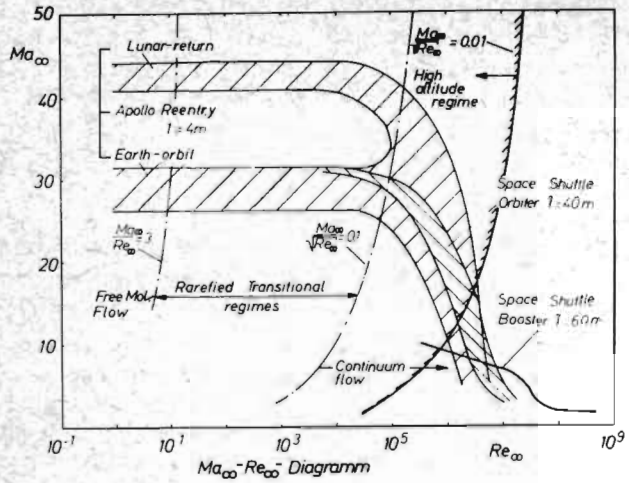


Fig. 2. Flight trajectories of typical re-entry vehicles (Mach-Reynolds-diagram)

The criterion

$$\frac{Ma_\infty}{\sqrt{Re_\infty}} \geq 0.01$$

characterizes the high altitude regime and it is seen from Fig. 2, that this criterion corresponds in terms of decreasing altitude to the occurence of transition from laminar to turbulent boundary layer. Deviations from the continuum flow regime begin for $Ma_\infty/\sqrt{Re_\infty} > 0.1$. In the transitional regime viscous effects become predominating and the boundary layers grow larger and larger and finally disappear. With diminishing density the collisions between the molecules decrease considerably and after all in the free molecular flow regime, which may be characterized by $Ma_\infty/Re_\infty > 3$ no collisions between the molecules occur in the flow field.

## 2.2 Inviscid hypersonic flow

### 2.2.1 Mach number independence principle and hypersonic similarity law

The density ratio across a shock wave

$$\varepsilon = \frac{\rho_\infty}{\rho_2} = \frac{\gamma-1}{\gamma+1}\left(1 + \frac{2}{C^2(\gamma-1)}\right) \qquad (1)$$

with $C = Ma_\infty \cdot \sin\sigma$ and $\sigma$ = shock wave angle tends to a limiting value

$$\varepsilon \sim \varepsilon_{lim} = \frac{\gamma-1}{\gamma+1}$$

with increasing $C$. In order that the flow field may be independent of the free stream Mach number $Ma_\infty$ it is necessary that at any point on the shock the density ratio $\varepsilon$ be independent of $Ma_\infty$; this leads to the conclusion

$$\frac{2}{C^2(\gamma-1)} \ll 1 .$$

For slender bodies in hypersonic flow a similitude law has been established which considers two flows as equivalent, if both are given by the same solution of the small disturbance equations. If the contour of both two dimensional bodies is given by

$$h(x) = \tau\, q(x) \qquad (2)$$

with two different values of the parameter $\tau$, invariant equations are obtained with the reduced variables

$$X = x, \quad Y = \frac{1}{\tau} y, \quad U = \frac{1}{\tau^2}\left(\frac{u}{u_\infty} - 1\right), \quad V = \frac{1}{\tau}\frac{v}{u_\infty} .$$

### 2.2.2 Newtonian theory

Following Newton's hypothetical model the pressure coefficient on the surface is proportional to the square of the cosine of the angle between the wind velocity and the normal to the surface

$$c_p = \frac{p - p_\infty}{\frac{1}{2}\rho V^2} = 2\cos^2\delta . \qquad (3)$$

In the case of $\delta = 90^\circ$ this formula should be identical with the pressure relation behind a normal shock

$$c_{ps} = \frac{2}{\gamma Ma_\infty^2}\left[\left(\frac{\gamma+1}{2} Ma_\infty^2\right)^{\frac{\gamma}{\gamma-1}} \cdot \left(\frac{\gamma+1}{2\gamma Ma_\infty^2 - \gamma + 1}\right)^{\frac{1}{\gamma-1}} - 1\right] . \qquad (4)$$

However $c_{ps} = 2$ only in the limiting case $Ma_\infty \to \infty$ and $\gamma \to 1$. On a purely empirical basis LEES [1] has proposed to use in the case of $\gamma \neq 1$ the formula

$$c_p = c_{ps}\cos^2\delta \qquad (5)$$

where for blunt bodies $c_{ps}$ is given by the formula (4) (modified Newtonian theory).

## 2.3 Viscous effects

The high temperatures encountered at hypersonic speeds behind the shock or in the boundary layer result in an increase of boundary layer thickness, which generates itself a hypersonic shock layer from the leading edge. The vorticity in the inviscid layer due to the curved shock wave is of the same order as the average vorticity in the boundary layer due to the shear stress.

2.3.1 Flat plate

The pressure distribution along a sharp-nosed flat plate is approximately proportional to the parameter $\chi = Ma_\infty^3 \sqrt{C}/\sqrt{Re_x}$, where $c = \mu T_\infty/\mu_\infty T$ and $Re_x = V_\infty x/\nu_\infty$ as is shown in Fig. 3 for the insulated flat plate in air. With heat transfer the slope of the curve is lower for a colder wall and higher for a hot wall.

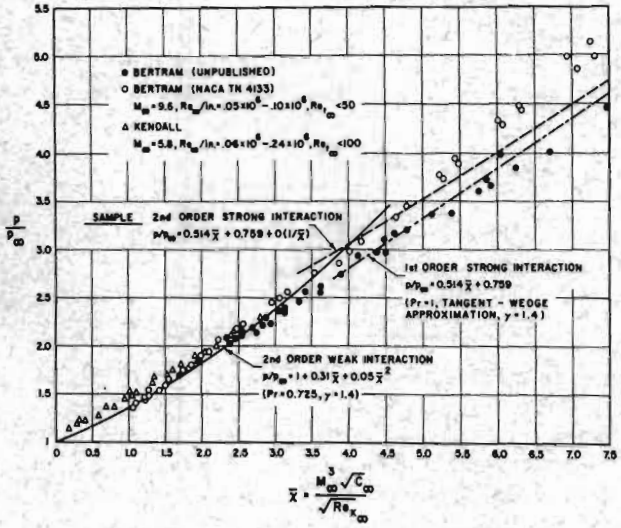


Fig. 3. Weak and strong interaction pressure results on an insulated flat plate in air [2]

2.3.2 Second order boundary layer theory

With diminishing Reynolds number the classical boundary layer theory must be modified to include secondary effects resulting from curvature (longitudinal and transverse), displacement, external vorticity (due to gradients of entropy or total enthalpy), slip and temperature jump. Dimensional analysis [3] shows, that the flow fields depend on the parameter

$$\varepsilon = \frac{\left[(\gamma - 1) Ma_\infty^2\right]^{\omega/2}}{\sqrt{Re_\infty}}$$

when the viscosity is assumed to be proportional to a power $\omega$ of temperature.

Approximate solution of the second order boundary layer equations have been obtained by DEVAN [4] and solutions were also calculated for separated flow past a bluff body [5]. A higher order theory for turbulent boundary layers was established for moderately large Reynolds numbers by AFZAL [6].

2.3.3 Free molecular flow

Free molecular flow is characterized by such a degree of rarefaction that intermolecular collisions are negligible. Thus in the flow field only undisturbed molecules, coming from infinity, and molecules reflected from the wall, are present. The reflection of the molecules may be specular or diffuse and the accommodation coefficients indicate that part of the molecules which is reflected diffusively.

For bodies with single reflection at the wall (convex curvature) simple formulas are obtained for the normal and tangential momentum which in the hypersonic limit take the form

$$p = \rho V^2 \left[(2 - \sigma') \cos^2 \delta + \frac{\sigma'}{2} \sqrt{\frac{2\pi T_w}{\gamma T}} \frac{\cos \delta}{Ma_\infty}\right] \quad (6)$$

$$\tau = \sigma \rho V^2 \sin \delta \cos \delta \,, \quad (7)$$

where $\sigma$ is the accommodation coefficient for tangential momentum and $\sigma'$ for normal momentum. Obviously the pressure force is composed of a temperature independent part, which is identical with the Newtonian force for diffuse reflection, and a temperature dependent part. The friction force is not influenced by wall temperature.

In the case of multiple reflection (bodies with concave curvature, wing-body configurations or interaction of separate bodies) the solution of an integral equation is required. It has been solved for different problems (flow in cylindrical or conical tubes, interaction of a wall with a cone), but for more general cases a numerical procedure is needed.

2.3.4 Monte-Carlo technique

The gas dynamics of the transitional flow regime between continuum flow and free molecular flow is described by the Boltzmann equation, which unfortunately cannot be solved by analytical methods. Among the different approximative methods the "direct simulation Monte-Carlo method" seems to be most promising. In this method proposed by BIRD [7, 8] the flow field is divided into a large number of cells. A multitude of molecules is supposed to be in each cell and the motion and collision data of the molecules are calculated and stored in an efficient computer. Results were obtained for bodies of simple shape. In Fig. 4 the calculated drag coefficient of a strip in transverse flow is compared with measurements [9] and Fig. 5 shows a comparison of Monte-Carlo data for a cylinder in cross flow with measurements by KOPPENWALLNER [10].

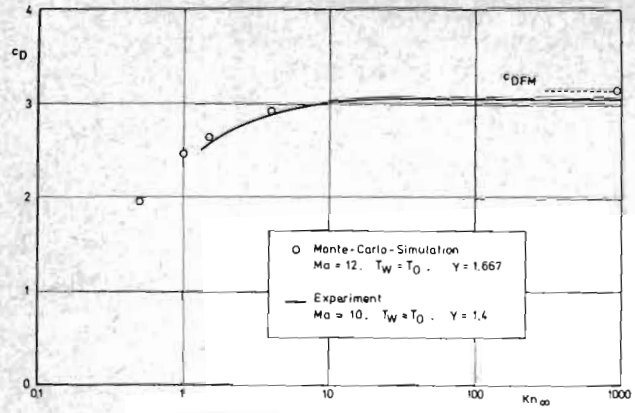


Fig. 4. Comparison of drag data for a strip calculated by Monte-Carlo technique with measured values

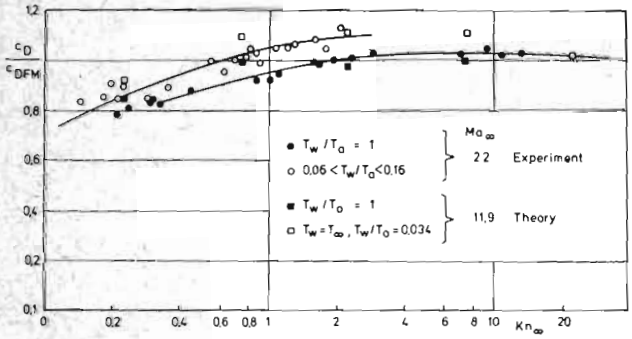


Fig. 5. Comparison of drag data for cooled and uncooled cylinders calculated by Monte-Carlo technique with measured values

## 2.4 Wind-tunnel experiments

As is shown in Fig. 2, for a rather complete simulation of reentry trajectories an extended range of Mach and Reynolds numbers is needed. Different types of wind tunnels are required to cover almost the whole range. As an example Fig. 6 shows the operational range of the hypersonic tunnels at the DFVLR-Aerodynamische Versuchsanstalt Göttingen, Germany, the Ludwieg-Tube-Tunnel, the Hypersonic-Low-Density-Tunnel with the closed wall test

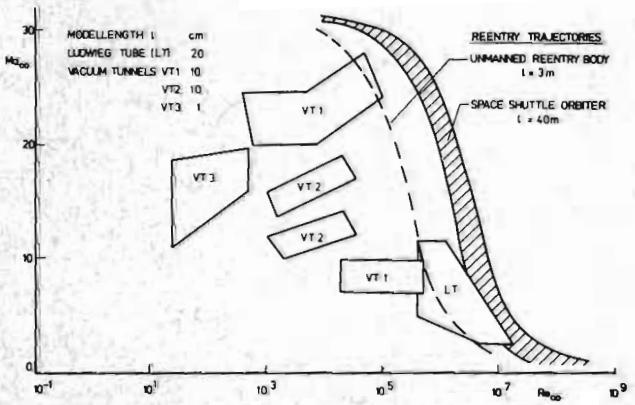


Fig. 6. Operational range of the hypersonic tunnels at the DFVLR-Aerodynamische Versuchsanstalt Göttingen, Germany

sections I and II and the free jet tunnel III. The Reynolds numbers are referred to the actual model sizes.

Conical nozzles are often used in hypersonic test sections because of simple manufacturing. In the influence region of the nozzle one has therefore a conical flow and from the continuity equation follows

$$\rho v = \frac{\text{const}}{r^2} \tag{8}$$

and as the velocity for expansion into vacuum reaches a limiting value, one obtains for suffiently large r

$$\rho = \frac{\text{const}}{r^2} \tag{9}$$

Corrections for the radiality of the flow and the variation of density must be applied.

### 2.4.1 Force measurements on simple shapes

Force measurements have been undertaken on simple shapes in the whole range from continuum flow to the free molecular flow. The results of Fig. 7 show a remarkable difference between the drag data of the uncooled and the cooled cylinder (10)

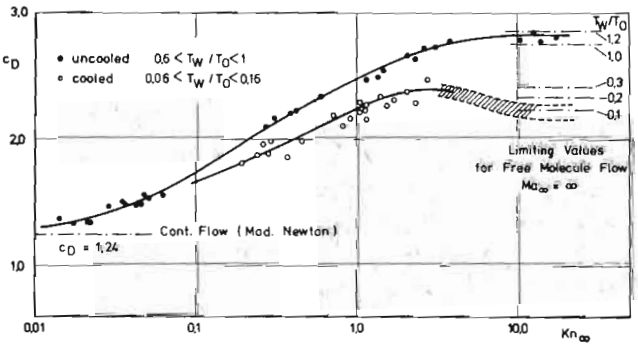


Fig. 7. Measured drag coefficient for uncooled and cooled cylinders in transitional flow

Whereas in the first case the free molecular limit is reached monotonically, in the latter case the drag coefficient has a maximum near a Knudsen number Kn = 3 . By subtracting the pressure drag it is shown in Fig. 8, that this behaviour is due to the friction drag, which has a maximum also for the uncooled cylinder. This behaviour may be compared with the flow of a rarefied gas through a tube, where KNUDSEN (11) has found a minimum of flow rate (known as "Knudsen minimum") which corresponds to a maximum of friction. An overshoot of drag coefficient is also predicted for very slender cones. In the cone data of Fig. 9 the cone angle is too large to show an overshoot (12). Cone drag measurements in free molecular flow (Fig. 10) are in close agreement with theoretical predictions for varying temperatures.

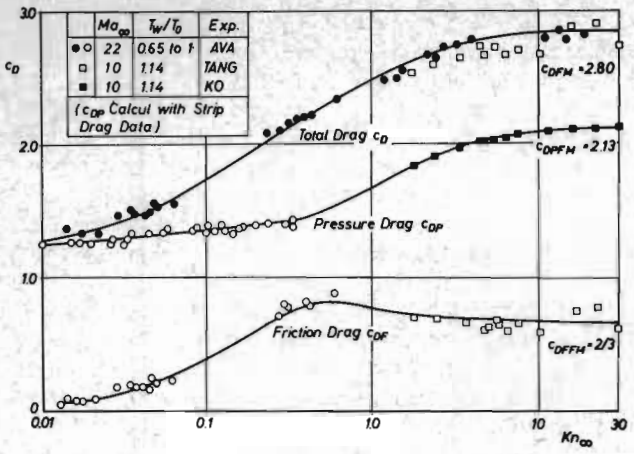


Fig. 8. Partition of total drag of uncooled cylinders in transitional flow regime into pressure drag and friction drag

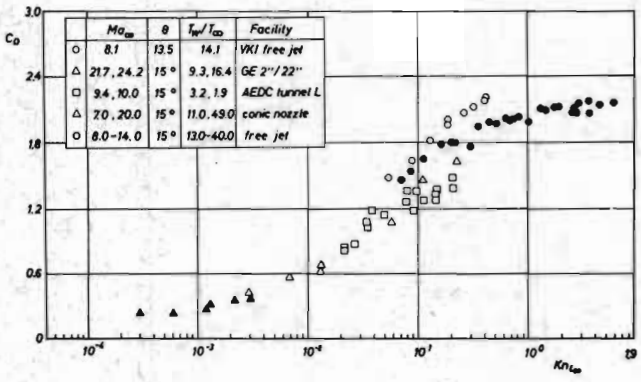


Fig. 9. Comparison of experimental cone data[12]

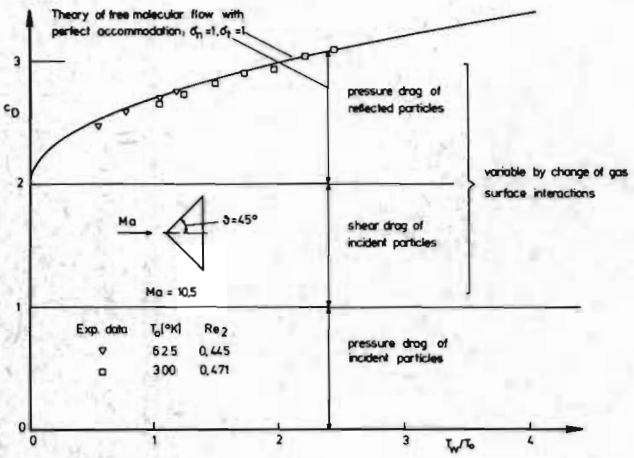


Fig. 10. Experimental cone drag data in free molecular flow for varying wall temperatures (by H. Legge unpublished)

## 2.4.2 Force measurements on reentry bodies

Drag measurements on the Apollo Command Module (Fig. 11) cover the whole range from free molecular flow to continuum flow [13]. The normal force coefficients of the blunt nosed Apollo CM is strongly dependent on Mach- and Reynolds number (Fig. 12) and may be represented as function of the rarefaction parameter $Ma_\infty/\sqrt{Re_\infty}$. A quite different behaviour is shown for lifting reentry bodies, where the normal force coefficient is nearly independent of Mach- and Reynolds number in the range $10 < Ma < 21$ and $10^3 < Re < 10^6$ (Fig. 13) [14]. The same is not true for the drag and the lift to drag ratio as is shown in Fig. 14, and the maximum values may again be represented as function of the rarefaction parameter $Ma_\infty/\sqrt{Re_\infty}$. The moment, too, depends on rarefaction.

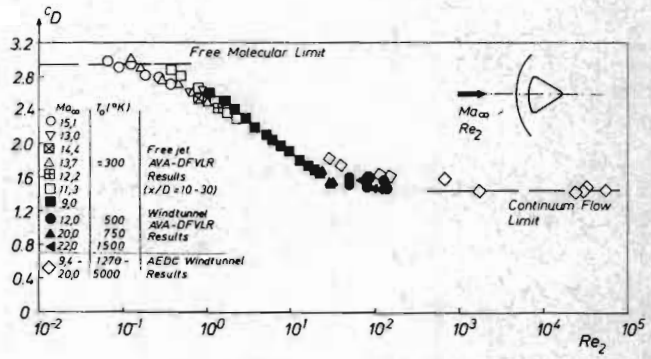


Fig. 11. Apollo Command Module drag coefficien in the range between continuum and free molecular flow [13]

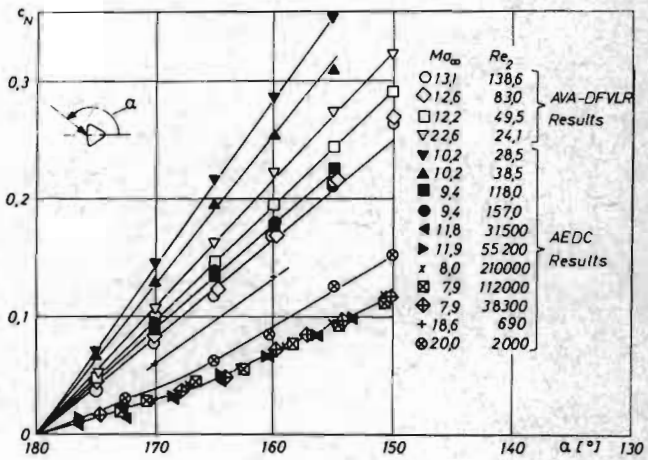


Fig. 12. Normal force coefficients of the Apollo Command Module at various Reynolds numbers [13]

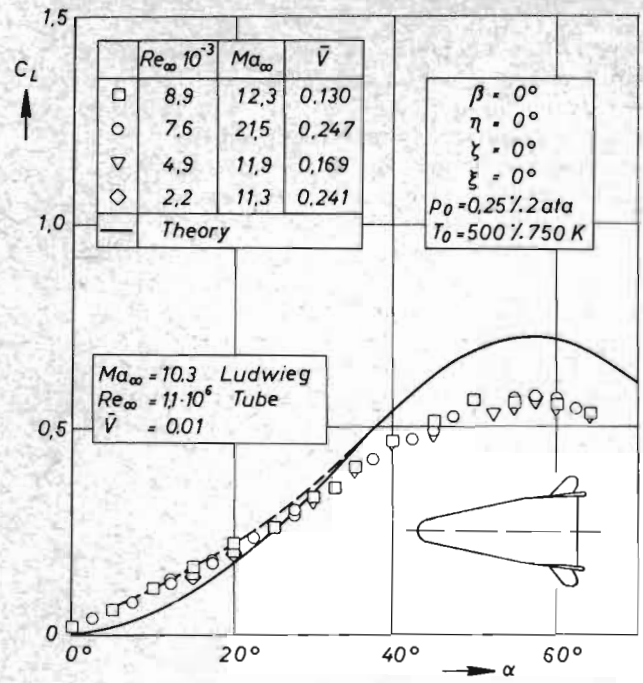


Fig. 13. Lift coefficient of lifting re-entry body as function of incidence angle at various Mach- and Reynolds numbers (14)

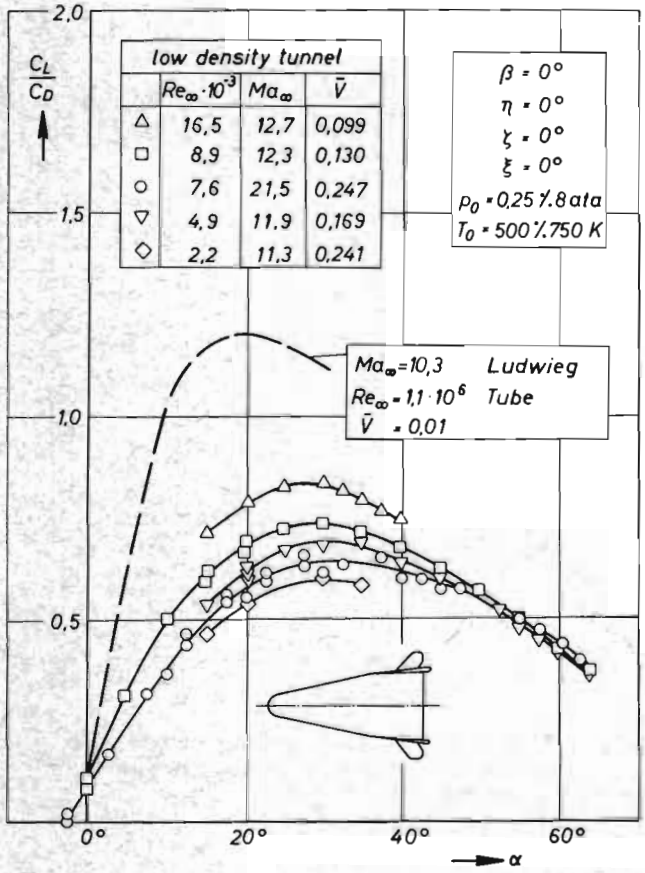


Fig. 14. Lift to drag ratio of lifting re-entry body as function of incidence angle at various Mach- and Reynolds numbers (14)

## 2.4.3 Heat transfer measurements

Heat transfer may be characterized by a Nusselt number, which corresponds to the ratio of the actual heat flux to the possible convective flux in still air, or by a Stanton number, which corresponds to the ratio of the actual heat flux to the total heat flux, oncoming in the frontal area. The Stanton number tends to unity in the limit of free molecule flow and may therefore be preferred in hypersonic rarefied flow (15). This is shown in Fig. 15 for the heat transfer on a sphere in hypersonic rarefied flow (16). The heat transfer distribution on a lifting reentry body is in a wide range independent from Mach and Reynolds number when it is normalized with the stagnation point heat transfer (Fig. 16).

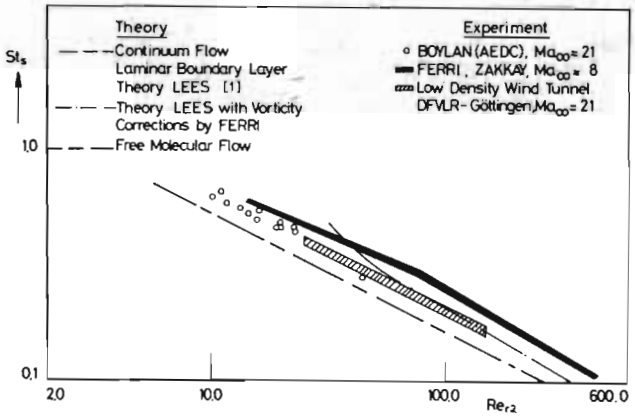


Fig. 15. Heat transfer in the stagnation point of a sphere. (Theories and experiments) (16)

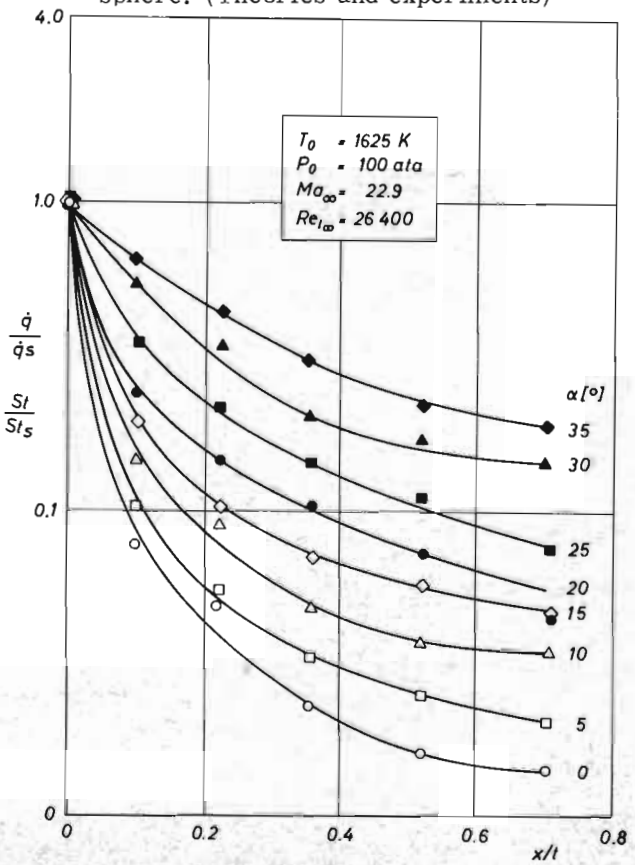


Fig. 16. Normalized heat transfer distribution along the center line of a re-entry body at different incidence angles (16)

## 2.5 Free flight tests

Only rare data are available which were obtained in free flight tests.

### 2.5.1 High Reynolds number tests

Slab delta wings and caret wings were investigated at the Woomera rocket range. A general description of the rocket-propellet free-flight model technique is given in Ref. [17] and a more detailed description of the method used to obtain heat-transfer data in Ref. [18]. Typical results of the slab delta wing tests [19] are plotted in Fig. 17 and 18. The Reynolds number referred to the length $l$ (see Fig. 17) was approximately $1.5 \cdot 10^7$, the altitude was below 20 km. The spanwise pressure distribution follows rather closely the modified Newtonian theory. The heat transfer rate to leading edge in dependence of Mach number follows more turbulent theory as could be expected and has a maximum at the geometric stagnation line.

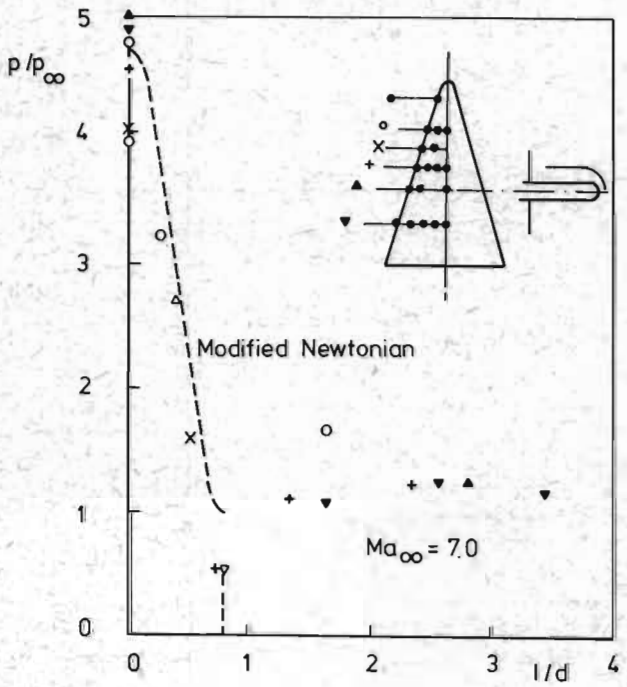


Fig. 17. Spanwise pressure distribution on a slab delta wing in free flight [19]

The free flight measurements on sharp [20] and blunt [21] leading edge caret wings were performed in a lower Mach number range up to 3.6 or respectively 3.36 and at altitudes below 1 km.

Fig. 19 gives a comparison of spanwise pressure distribution for free flight tests on sharp and blunt caret wings and wind tunnel tests on sharp wings. Obviously there is a good agreement. The heat transfer data for the blunt wing (Fig. 20) follows closely turbulent theory by BECKWITH and GALLAGHER [22].

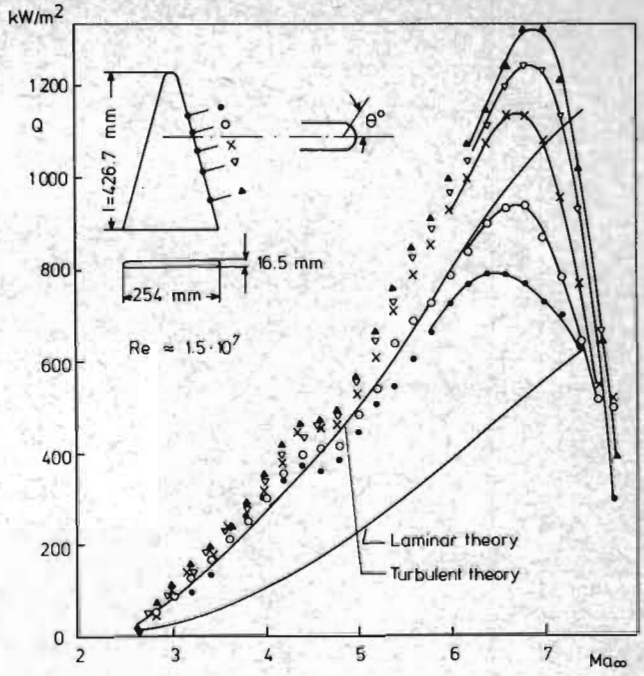


Fig. 18. Heat transfer rate to leading-edge geometric stagnation line ($\theta = 0$) of a slab delta wing in accelerating free flight for different Mach numbers [19]

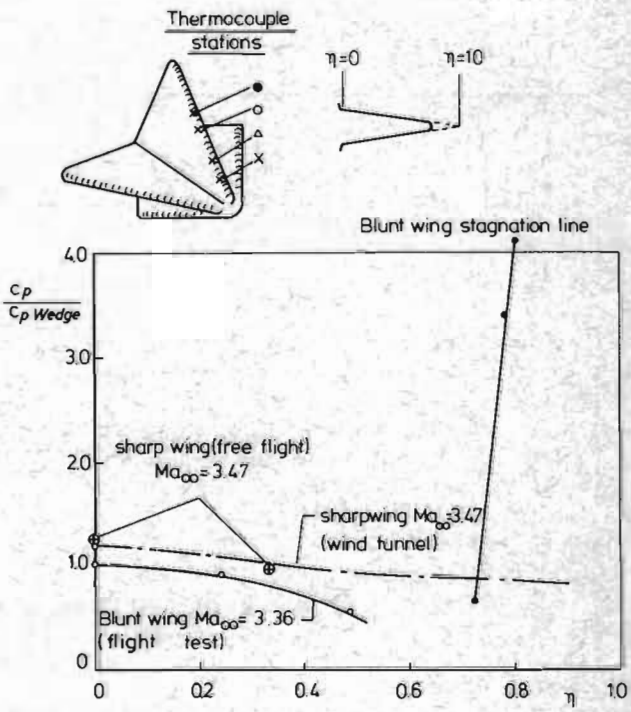


Fig. 19. Pressure distribution on sharp and blunt caret wing in free flight compared with wind tunnel measurements [21]

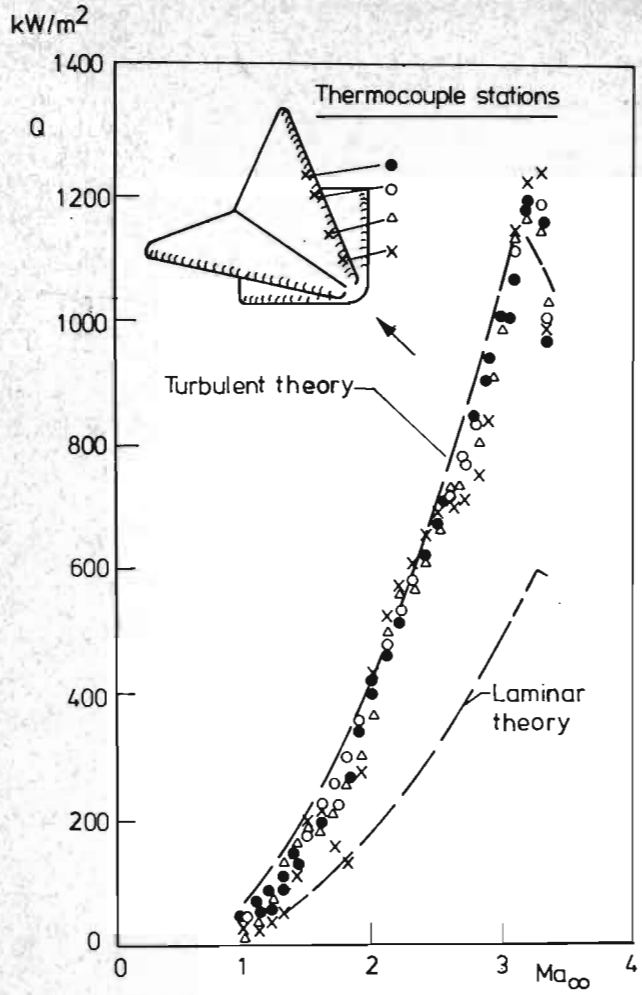


Fig. 20. Heat transfer to leading-edge nominal stagnation line of a blunt caret wing in accelerating flight [21]

2.5.2 Low Reynolds number tests

A comparison of flight and wind tunnel test data are available for the Apollo Command Module [23]. A summary of lift to drag and trimangle data is given in Fig. 21. However flight data exist only for Reynolds numbers superior to $7 \cdot 10^3$. From the good agreement between wind tunnel data, where real gas effects were not simulated, and full-scale flight data, where real gas effects were present, it may be concluded, that real gas effects are not significant on the static stability of the Apollo Command Module.

A series of rocket launched flights are being undertaken to provide heat transfer measurements to hemisphere and bluff cylinders in actual high altitude flight conditions [24]. This will provide a basis for a comparison of free flight and wind tunnel data.

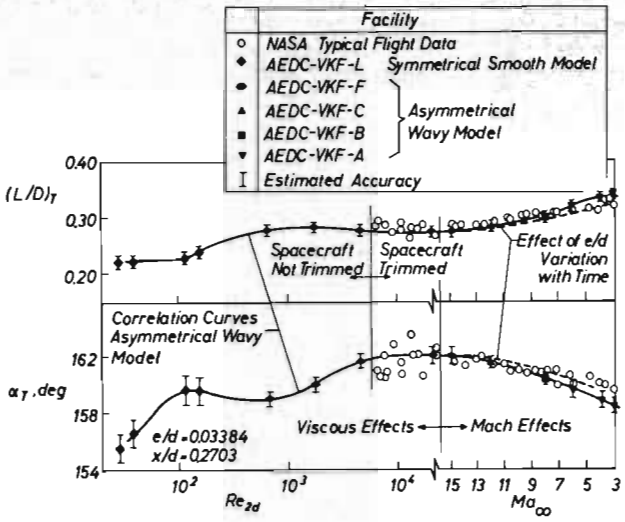


Fig. 21. Free flight and wind tunnel tests an Apollo Command Module. Summary of lift to drag ratio and trim angle [23].

## 3. High enthalpy simulation

### 3.1 Thermodynamics of high enthalpy flow

The thermodynamic conditions of a gas at high temperatures is determined by the number of degrees of freedom. In thermodynamic equilibrium each degree of freedom contains the same amount of energy $kT/2$. At high enthalpy the thermodynamic properties of real air deviate from an ideal gas with constant specific heats. These deviations result from various physical processes namely vibrational excitation, chemical reactions and ionisation. Fig. 22 shows the composition of air in equilibrium for varying temperatures.

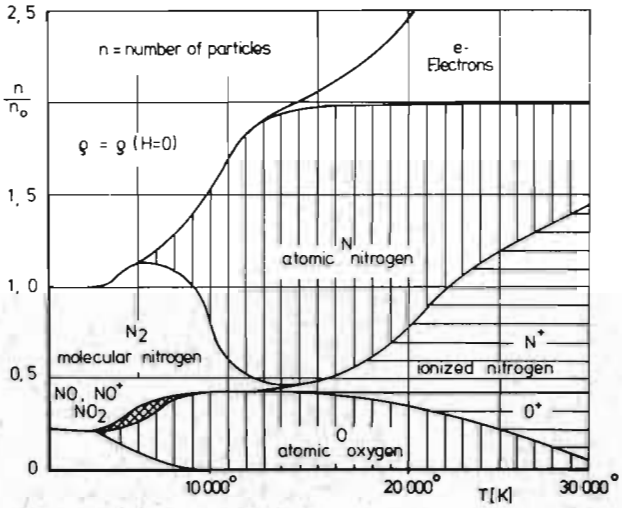


Fig. 22. Composition of air at high temperatures

### 3.2 Real gas relaxation [25, 26]

Energy changes occur at finite rates, which can be characterized by relaxation times, or by a relaxation length in a flow of given velocity. If all relevant relaxation lengths are very much shorter than the smallest flow field dimension of interest, the flow may be regarded as being in thermodynamical equilibrium. If relaxation lengths and flow field dimensions are comparable, the resulting nonequilibrium real gas effects may greatly influence aerodynamic properties. If all relevant relaxation length are very much greater than the largest flow field dimension of interest, the flow may be regarded as being frozen, so that its vibrational energy, chemical composition and degree of ionisation remain constant. In this situation air may again be treated as a perfect gas with constant specific heats.

For conditions generated in flight at less than about 6 km/s , six elementary processes are adequate to describe chemical changes in the high temperature region behind a bow shock in pure air. At higher velocities charge transfer reactions such as

$$N_2 + NO + \rightleftharpoons N_2^+ + NO$$

becomes progressively more important and 54 elementary reactions are then required for an adequate description of chemistry and ionisation history of the air flow [26]. It is generally not possible to study all these processes in detail, and an empirical relaxation time for dissociation is introduced, based on the approach to equilibrium of the temperature T in the non-equilibrium flow behind a normal shock wave.

HARNEY [25] has established a dividing line between the regimes of "chemical effects negligible" and "nonequilibrium chemistry" based on the criterion that no more than 10 percent of the oxygen is dissociated over the flow region of interest. Two different flow regions of interest representing two characteristic flight configurations are considered, namely the nose region of an axisymmetric body with a nose radius of 0.3 m and a 45 deg planar shock as representative of the flow on the windward side of a winged body at an angle of attack. The chart has been extended by indicating the regime of vibrational nonequilibrium, using as limits the conditions that the vibrational relaxation length behind a normal shock lies between 0.01 and 1.0 m . Also lines of rotational and translational relaxation are indicated corresponding to the conditions that $3\lambda = 0.1$ m oder $10\lambda = 0.1$ m , where 0.1 m is taken as approximate stand-off distance of the shock wave on a blunt body with 0.3 m curvature radius (Fig. 23).

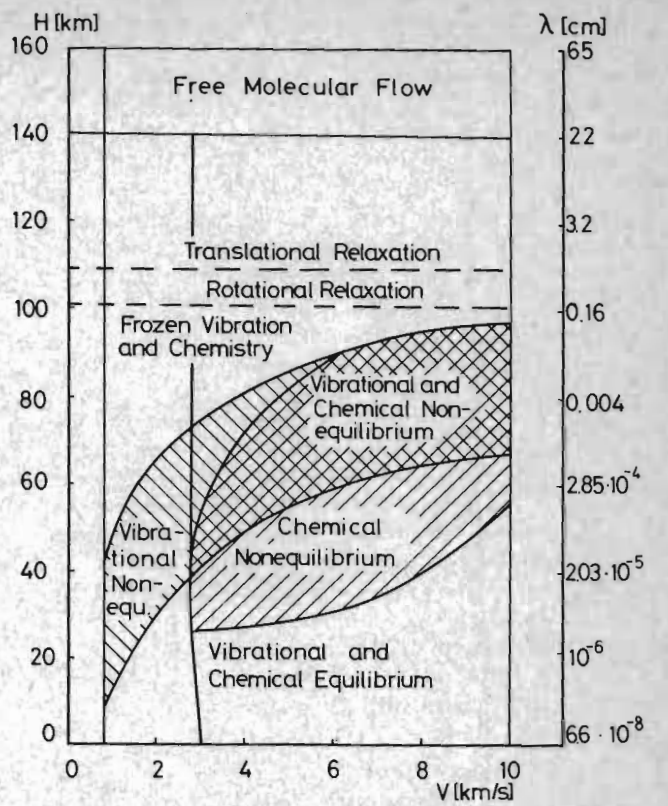


Fig. 23. Different regimes of relaxation phenomena in hypersonic rarefied flow for a blunt nosed body with curvature radius of 0.3 m

### 3.3 Real gas effects on lifting re-entry aerothermodynamics

As the velocity and altitude of a re-entry vehicle decreases it will generally pass through the regime of frozen low density flow at high altitude, nonequilibrium at lower altitude and equilibrium real gas flow at low altitude, if the flight trajectory includes a sufficiently high velocity. A re-entry vehicle, like the space shuttle, being a large and complex shape, has many characteristic lengths and so the boundaries between the different regions are necessarily diffuse.

LORDI, VIDAL and JOHNSON [27] have calculated the chemical nonequilibrium effects on the flow in the windward plane of symmetry of a blunted orbiter and presented results for different streamlines. The following conclusions are drawn by BRAY [28] from this calculations and other investigations:

a) Nonequilibrium gas effects are to be expected at least within the altitude range 60 - 75 km .

b) The occurrence of thick boundary layers and consequently significant viscous/inviscid flow interaction phenomena is promoted by the swallowing of the nonequilibrium entropy layer.

c) The distance of the transition point from the leading edge is found to move upstream by a factor of between 2.5 and 4 , if the non-equilibrium entropy layer is taken at the boundary edge. Further departure from equilibrium leads to a prediction of earlier transition.

d) The laminar heat transfer in the nose region will be reduced considerably (about 40 %) below the chemical equilibrium value if the boundary layer is frozen while the effect on the after body is expected to be less.

e) Inviscid nonequilibrium flow phenomena have only a very small effect on the pressure distribution, and hence on the lift, drag and pitching moment, for slender, flat-bottomed deltas [29]. These effects are considerably larger for caret wings, where nonequilibrium flow can cause a fall in pressure of up to about 20 % as the flow approaches equilibrium.

f) The level of ionisation in the shock layer is strongly influenced by nonequilibrium effects with important implications for radio communications.

### 3.4 Wind tunnel simulation of high enthalpy flow

Wind tunnel simulation of high enthalpy flow is faced with two severe barriers:

1) Enormous values of reservoir pressure $p_o$ and reservoir temperature $T_o$ are required to duplicate flight conditions. This may be seen from Fig. 24.

2) During expansion of the test gas in the wind tunnel nozzle departure from vibrational and chemical equilibrium occurs and the medium does not properly represent the thermodynamic properties of atmospheric air. For extremely low density in high vacuum tunnels this is even valid for the translational energy, where the longitudinal component freezes during expansion.

In the absence of complete duplication of flight conditions, wind tunnel tests must resort to one or more of the following possibilities:

1. Nonsimulation

   The test conditions which are known to be unrepresentative of flight conditions are compared with corresponding computations. Real flight conditions are obtained by theoretical extension of nonequilibrium results.

For this procedure an extensive development of theoretical analysis is needed.

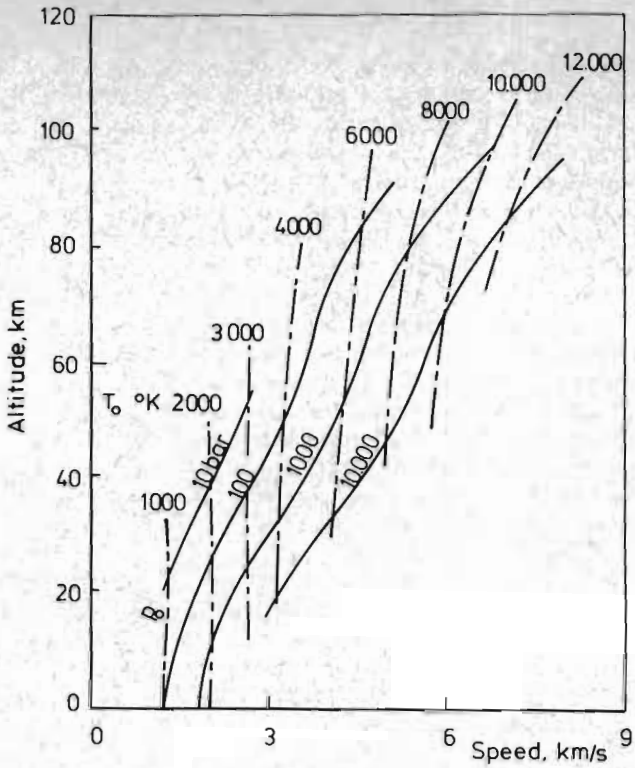


Fig. 24. Wind tunnel reservoir conditions for flight duplication according to BRAY [26]

2. Partial simulation

Not all of the similarity parameters of the flight situation are properly matched but conditions are choosen, which minimise the resulting errors (see Ref. [30]).

3. Correct simulation of only a part of the non-equilibrium flow field

This method has been applied to simulate stagnation point heat transfer in shock tubes and electric arc flows.

In existing hypersonic facilities one tries to duplicate either Mach- and Reynolds number or to simulate only a part of the nonequilibrium flow field. To the first group belong hypersonic low density tunnels with rather high reservoir pressure and hypersonic Ludwieg tubes, to the latter group shock tubes, hotshots and supervelocity free flight ranges. Wind tunnels which give neither a correct simulation of the high enthalpy flow field nor a Mach-Reynolds number duplication are only of limited value. To this group belong arc-heated continuously operating low density tunnels with low reservoir pressure, sometimes incorrectly named Plasma tunnels.

## 4. Conclusions

The following conclusions may be drawn from the results of this investigation.

1. It is possible to investigate in existing facilities the rarefaction effects on simple shapes in the whole range from continuum flow to free molecule flow which comprises three of four decades of Reynolds number. Correct wind-tunnel simulation of the complete non-equilibrium flow field past lifting re-entry vehicle shapes under conditions of interest appears to be impossible at the present time. Techniques involving incomplete simulation must be employed.

2. Further theoretical study is required of both inviscid and viscous nonequilibrium flows past complex three dimensional shapes.

3. The forces acting upon a body in hypersonic flow result from the pressure force of the incident particles (which corresponds to Newtonian force), the pressure force of the reflected particles, which depends on wall temperatures and the friction force, which is relatively small in the continuum limit and reaches a constant value in the free molecular limit after passing a maximum.

4. The normal force coefficient of lifting bodies is only slightly influenced by Mach- and Reynolds number in the range $10 < Ma < 20$ and $10^3 < Re < 10^6$. The normal force coefficient of blunted bodies (e.g. Apollo CM) is strongly influenced by Mach- and Reynolds number and may be represented as function of the rarefaction parameter $Ma_\infty \sqrt{Re_\infty}$.

5. The drag forces of blunt bodies and lifting re-entry bodies are a function of the rarefaction parameter $Ma_\infty \sqrt{Re_\infty}$. Bodies with predominant friction force (e.g. strongly cooled bodies) reach a maximum drag coefficient in transitional regime.

6. The moment coefficient of lifting re-entry bodies is much influenced by boundary layer shock interference. Newtonian theory is not appropriate to describe the measured data.

7. It is preferable to characterize heat transfer data by a Stanton number, because it tends to unity in the limiting case of free molecular flow. Existing theories are in close agreement with measurements on simple shapes and lifting re-entry bodies.

8. Departure from equilibrium, which is at least to be expected within the altitude range 60 - 75 km has a predominant influence on the boundary and entropy layer, on transition and heat transfer.

9. Inviscid nonequilibrium flow phenomena have only a very small effect on the pressure distribution of slender flat-bottomed deltas but a large effect for caret wings.

## 5. References


(1) LEES, L., Hypersonic Flow. Proc. 5th Intern. Aero. Conf., Los Angeles, Inst. Aero. Sci., New York, 241-276, 1955.

(2) HAYES, W.D., PROBSTEIN, R.R., Hypersonic Flow Theory. Applied Math. and Mech., Vol. 5, 1959.

(3) Van DYKE, M., Higher Order Boundary Layer Theory. Annual Rev. Fluid Mech., Vol. 1, 265-292, 1969 Annual Reviews, Inc., U.S.A.

(4) DEVAN, L., Approximate Solution of Second Order Boundary Layer Equations. AIAA J. 3, No. 12, 1965, 2197-2202.

(5) BLUSTON, H.S., PANTSON, R.W., A Second Order Boundary Layer Solution for Separated Flow Past a Bluff Body. ZAMP 24, 1973, 488-498.

(6) AFZAL, Noor, A Higher Order Theory for Compressible Turbulent Boundary Layers at Moderately Large Reynolds Numbers. J. Fluid Mech. 57, 1973, Nr. 1, 1-25.

(7) BIRD, G.A., Aerodynamic Properties of Some Simple Bodies in the Hypersonic Transition Regime. AIAA J., Vol. 4 (1966) No. 1.

(8) BIRD, G.A., The Structure of Rarefied Gas Flows Past Simple Aerodynamic Shapes. J. Fluid Mech., Vol. 36, 1969, No. 3.

(9) BOETTCHER, R.-D., Monte-Carlo Simulation der hypersonischen verdünnten Strömung um einen querangeströmten Streifen. Int. AVA-Ber. 71 A 20, Göttingen, 1971.

(10) KOPPENWALLNER, G., Experimentelle Untersuchung der Druckverteilung und des Widerstandes von querangeströmten Kreiszylindern bei hypersonischen Machzahlen. Z. Flugwiss. 17 (1969), 321-332.

(11) KNUDSEN, M., Die Gesetze der Molekularströmung und der inneren Reibungsströmung der Gase durch Rohre. Ann. d. Physik 28, 1909, 75-130.

(12) LEGGE, H., Drag Measurements of Cones at Zero Angles of Attack in Near Free Molecular Flow. DLR-FB 72-64, 1972.

(13) KOPPENWALLNER, G., LEGGE, H., MÜLLER, H., Apollo Command Module Aerodynamic Simulation Tests in Hypersonic Flow. DLR-FB 71-83, 1971.

(14) BÜTEFISCH, K.A., SCHÖLER, H., Windkanalmessungen an einem Raumflugkörper in verdünnter Hyperschallströmung. Raumfahrtforschung, Vol. 18, 1974, 1, 10-16.

(15) VENNEMANN, D., BÜTEFISCH, K.A., Über die Verwendung temperaturempfindlicher Kristalle bei aerodynamischen Untersuchungen. DLR-FB 73-121, 1973.

(16) KOPPENWALLNER, G., VENNEMANN, D., Wärmeübergangsmessungen an einem Modell des ERNO-Lifting Body LB 21. Int. AVA-Ber. 063-72 H 03, Göttingen, 1972.

(17) HAMILTON, J.A., Free Flight Techniques for High Speed Aerodynamic Research. J. Roy. Aeronaut. Soc., Vol. 60, 1956, 151-177.

(18) PICKEN, J., WALKER, D., Techniques for the Investigation of Aerodynamic Heating Effects in Free Flight. AGARD Rep. 376, 1961.

(19) GREENWOOD, G.H., Free-Flight Measurements of Pressure and Heat Transfer on a Slab Delta Wing at Mach Numbers Between 2.6 and 7.75. RAE Tech. Rep. 70169, 1970.

(20) PICKEN, J., GREENWOOD, G.H., Free Flight Measurements on Heat Transfer and Observations of Transition on a Caret Wing at Mach Numbers up to 3.6 . RAE Tech. Rep. 65237, 1965.

(21) GREENWOOD, G.H., Free Flight Measurements of Pressure and Heat Transfer on a Blunt Leading-Edge Caret Wing at Design and Off-Design Mach Numbers ($M_\infty$ = 0.9 to 3.36). R & M 3679, 45 pp., 1971.

(22) BECKWITH, I.E., GALLAGHER, J.J., Local Heat Transfer and Recovery Temperatures on a Yawed Cylinder at a Mach Number of 4.15 and High Reynolds Numbers. NASA Tech. Rep. R-104, 1961.

(23) GRIFFITH, B.J., BOYLAN, D.E., Postflight (AS-202) Apollo Command Module Aerodynamic Simulation Tests. AEDC-TR-67-238, 1968.

(24) METCALF, S.C., BERRY, C.J., COLEMAN, G.T., Heat Transfer to Bluff Faced and Hemispherical Faced Cylinders Between Continuum and Free Molecular Flow Limits. Pap. Pres. 9th Rarefied Gas Dynamics Symp., Göttingen, July 1974.

(25) HARNEY, D.I., Chemical Kinetic Regimes of Hypersonic Flight Simulation. AEDC-TDR-63-3, 1963.

(26) BRAY, K.N., Real Gas Effects on Lifting Re-Entry Aerothermodynamics. AGARD Lectures Series No. 42, Vol. 1, Lecture 9, 1972.

(27) LORDI, J.A., VIDAL, R.J., JOHNSON, C.B., Chemical Nonequilibrium Effects on the Flow in the Windward Plane of Symmetry of a Blunted Delta Orbiter. NASA TMX 2508, Dec. 1971.

(28) BRAY, K.N., Real Gas Effects During Space Shuttle Re-Entry. Meet. Aero. Res. Counc. Hypersonics Subcommittee, 18th July 1972.

(29) SQUIRE, L.C., A Comparison of the Lift of Flat Plate Delta Wings and Waveriders at High Angles of Incidence and High Mach Number. ARC 32555, 1970.

(30) WITTLIFF, C.E., SUNDARAM, T.R., A Study of Hypervelocity Slender-Body Flows and Similitudes Including the Effects of Nonequilibrium and Nose Bluntness. AIAA Paper No. 68-14, 1968.